HHS Public Access

Author manuscript

Mol Psychiatry. Author manuscript; available in PMC 2020 May 03.

Published in final edited form as:

Mol Psychiatry. 2020 May ; 25(5): 1006–1021. doi:10.1038/s41380-019-0506-1.

A POMC-originated circuit regulates stress-induced hypophagia, depression and anhedonia

Na Qu[1,4,8], **Yanlin He**[1,8], **Chunmei Wang**[1,8], **Pingwen Xu**[1], **Yongjie Yang**[1], **Xing Cai**[1], **Hesong Liu**[1], **Kaifan Yu**[1], **Zhou Pei**[1], **Ilirjana Hyseni**[1], **Zheng Sun**[2,3], **Makoto Fukuda**[1], **Yi Li**[4,5], **Qing Tian**[6], **Yong Xu**[1,7,*]

[1]Children's Nutrition Research Center, Department of Pediatrics, Baylor College of Medicine, One Baylor Plaza, Houston, TX 77030;

[2]Department of Medicine, Baylor College of Medicine, One Baylor Plaza, Houston, TX 77030;

[3]Shandong University Qilu Hospital, Jinan, Shandong, China;

[4]Affiliated Wuhan Mental Health Center, Tongji Medical College, Huazhong University of Science and Technology, Wuhan 430012, China;

[5]Research Center for Psychological and Health Sciences, China University of Geosciences, Wuhan 430074, China;

[6]Department of Pathology and Pathophysiology, School of Basic Medicine, Institute for Brain Research, Huazhong University of Science and Technology, Wuhan 430030, China;

[7]Department of Molecular and Cellular Biology, Baylor College of Medicine, One Baylor Plaza, Houston, TX 77030.

Abstract

Chronic stress causes dysregulations of mood and energy homeostasis, but the neurocircuitry underlying these alterations remain to be fully elucidated. Here we demonstrate that chronic restraint stress in mice results in hyperactivity of pro-opiomelanocortin neurons in the arcuate nucleus of the hypothalamus ($POMC^{ARH}$ neurons) associated with decreased neural activities of dopamine neurons in the ventral tegmental area (DA^{VTA} neurons). We further revealed that $POMC^{ARH}$ neurons project to the VTA and provide an inhibitory tone to DA^{VTA} neurons via both direct and indirect neurotransmissions. Finally, we show that photoinhibition of the $POMC^{ARH}\rightarrow$VTA circuit in mice increases body weight and food intake, and reduces depression-

*To whom correspondence should be addressed: Yong Xu, PhD & MD, 1100 Bates Street #8066, Houston, TX 77030, USA, Mail stop code: MCB320, yongx@bcm.edu, Ph: (713)798 7199, Fax: (713) 798 7187.

Author Contributions: N.Q., Y.H. and C.W. were involved in experimental design and most of procedures, data acquisition and analyses, and writing the manuscript. P.X, Y.Y., X.C., H.L., K.Y., Z.P. and I.H. assisted in production of study mice, surgical procedures and blinded evaluation of mouse behaviors. Z.S., M.F., Y.L, and Q.L. were involved in study design and writing the manuscript. Y.X. is the guarantor of this work and, as such, had full access to all the data in the study and takes responsibility for the integrity of the data and the accuracy of the data analysis.

[8]These authors contributed equally to this work.

The authors have no conflict of interest to disclose.

Disclosure summary: The authors have nothing to disclose.

like behaviors and anhedonia in mice exposed to chronic restraint stress. Thus, our results identified a novel neurocircuitry regulating feeding and mood in response to stress.

Keywords

POMC; dopamine; GABA; MOR; food intake; depression; stress

Introduction

Stress is a physiological and adaptive response to changes in the environment, but can also cause pathological alterations. For example, chronic stress increases vulnerability to anxiety, depression and other mood disorders[1]. In addition, stress is also known to change feeding behavior and energy homeostasis[2–4]. However, the neurocircuitry underlying stress-induced alterations in mood and energy balance is not fully understood.

The ventral tegmental area (VTA) in the midbrain is one main brain region that responds to various aversive stimuli and coordinates behavioral and metabolic adaptations[5]. Heterogeneous neural types exist within the VTA, including about 65% dopamine (DA) neurons, 30% GABAergic neurons, and 5% glutamatergic neurons[6–8]. In particular, depression-like behavior in animals is associated with reduced DA bioavailability[9], and antidepressant treatment increases DA transmission[10]. Optogenetic activation of DA^{VTA} neurons in mice reduces anhedonia and depression-like phenotypes, as measured in a variety of behavioral assays, including the sucrose preference test (SPT), the forced swim test (FST) and the tail suspension test (TST)[11, 12]. Further, a step-like stimulation of DA^{VTA} neurons also increases sucrose preference in mice, although this manipulation does not significantly alter depression-like behaviors measured by FST and TST[13]. Leptin, the anorexigenic hormone, has been reported to act upon DA^{VTA} neurons to regulate mood[14–16]. DA^{VTA} neurons may also play essential roles in the regulation of food intake, as mice born without DA synthesis develop hypophagia which can be rescued by supplement with a DA analog[17, 18]. However, the role of DA^{VTA} neurons in feeding control appears to be complex, since chemogenetic activation of DA^{VTA} neurons increases meal frequency but reduces meal size, resulting in unaffected total food intake[19].

Pro-opiomelanocortin (POMC) neurons and agouti-related peptide (AgRP) neurons, both located within the arcuate nucleus of hypothalamus (ARH), play essential roles in feeding control[20–24]. In particular, $POMC^{ARH}$ neurons secret α-melanocyte-stimulating hormone (α-MSH) to stimulate melanocortin 3/4 receptor (MC3R/MC4R) and reduce food intake; on the other hand, AgRP inhibits MC3R/MC4R to increase feeding[20–22]. Notably, $POMC^{ARH}$ neurons also release another neuropeptide, β-endorphin, but its role in feeding control is debatable[25–28]. It has been reported that chronic restraint stress increases POMC gene expression in the ARH by about 60%[3], but functions of $POMC^{ARH}$ neurons in the context of chronic stress remains unclear.

In the current study, we first examined the neural activities of DA^{VTA} neurons, $POMC^{ARH}$ neurons and $AgRP^{ARH}$ neurons in mice exposed to chronic restraint stress, and observed increased $POMC^{ARH}$ neuron activity and decreased DA^{VTA} neuron activity. We further

identified a $POMC^{ARH}$→VTA circuit and systemically examined neurotransmissions between $POMC^{ARH}$ neurons and various types of VTA neurons. Finally, we tested the functional relevance of the $POMC^{ARH}$→VTA circuit in the regulations of feeding, anhedonia and depression-like behaviors in mice exposed to chronic restraint stress.

Results

Chronic restraint stress induces hypophagia, anhedonia and depression-like behaviors

We first examined effects of chronic restraint stress on energy balance, anhedonia and depression-like behaviors in mice. To this end, wild type mice (males, 3 months of age) were randomly divided into control (CON) and restraint (RST) groups. The RST mice were subjected to 1-hour restraint (9:30am-10:30am) every day for 14 consecutive days (Figure 1A), while the control mice were left intact. During the 14-day period, RST mice displayed significant reductions in their body weight (about 6–7 g) compared to CON mice which plateaued from day 8 (Figure 1B). Food intake was also significantly reduced in RST mice during the entire 14-day period (Figure 1C). These results are consistent with previous report[3] and indicate that chronic stress induces body weight loss presumably due to hypophagia.

We then examined the behavioral consequences in RST mice vs. CON mice after they completed the 14-day paradigm. Similar to observations reported previously[29], RST mice displayed anhedonia in a sucrose preference test (SPT) compared to CON mice (Figure 1D). Further, we observed significantly increased despair in RST mice, as demonstrated by increased immobility in both forced swim test (FST) and tail suspension test (TST, Figure 1E–F). Together, these results indicate that chronic stress results in depression-like behaviors.

Chronic stress leads to inhibition of DA^{VTA} neurons and activation of $POMC^{ARH}$ neurons

Since DA^{VTA} neurons play an essential role in regulating depression[11, 12], we sought to examine whether RST can regulate activity of DA^{VTA} neurons. To this end, DAT-CreER/Rosa26-LSL-tdTOMATO mice (after tamoxifen induction) were subjected to CON or RST paradigm for 1 day, 4 days or 14 days, and we recorded firing activity of DA^{VTA} neurons (TOMATO-labelled) in brain slices prepared from these mice immediately after they were exposed to RST or CON treatment (Figure 1G). We found that compared to CON mice, RST for 1 day significantly reduced the firing frequency of DA^{VTA} neurons but did not change their resting membrane potential; RST for 4 or 14 days produced similar inhibitory effects to significantly reduce firing frequency and resting membrane potential of DA^{VTA} neurons (Figure 1H–J and S1A–B). No significant changes were noted in the after-hyperpolarization (Figures S1C–D). Interestingly, RST failed to change firing frequency and resting membrane potential of DA neurons in the substantia nigra (Figure S1E–H).

Given the changes in body weight and feeding induced by RST, we speculated that RST may also influence activity of appetite-regulatory neurons, e.g. $POMC^{ARH}$ neurons and/or $AgRP^{ARH}$ neurons. Using POMC-CreER/Rosa26-LSL-tdTOMATO mice (after tamoxifen induction) subjected to CON or RST paradigm, we found that RST for 1 day significantly

increased the resting membrane potential of $POMC^{ARH}$ neurons but did not change their firing frequency; RST for 4 or 14 days produced similar excitatory effects to significantly increase firing frequency and resting membrane potential of $POMC^{ARH}$ neurons (Figure 1K–N and S1I–J). However, RST failed to significantly alter the firing activity of $AgRP^{ARH}$ neurons (TOMATO-labelled neurons in AgRP-IRES-Cre/Rosa26-LSL-tdTOMATO mice, Figure 1Q–R and S1K–L).

$POMC^{ARH}$ neurons inhibit DA^{VTA} neurons via direct and indirect neurotransmissions

Given the concurrent changes in activities of DA^{VTA} neurons and $POMC^{ARH}$ neurons in RST mice, we postulated that $POMC^{ARH}$ neurons may project to DA^{VTA} neurons to form a neural circuit. To test this possibility, we stereotaxically injected AAV-FLEX-Synaptophysin-GFP into the ARH of POMC-Cre mice to selectively express Synaptophysin-GFP in $POMC^{ARH}$ neurons (Figure S2A and S2B-left panel). We observed abundant GFP-labelled neural terminals and boutons in the VTA (Figure S2B-middle panel), indicating that $POMC^{ARH}$ neurons project to the VTA. Notably, while some of the GFP-labelled boutons were in close proximity to DA neurons (identified as TH-positive neurons), many GFP-labelled boutons appeared to form contacts with non-DA neurons in the VTA (Figure S2B-right panel). Further, we stereotaxically injected AAV-FLEX-GTB and EnvA G-deleted Rabies-mCherry viruses into the VTA of DAT-CreER mice for retrograde tracing from DA^{VTA} neurons (Figure S2C–S2D). We noted many mCherry-labelled neurons in the ARH, a portion of which were confirmed to be POMC neurons as demonstrated by co-staining of β-endorphin (Figure S2E). Notably, many mCherry-labelled ARH neurons were not POMC neurons (Figure S2E), indicating that DA^{VTA} neurons also receive synaptic inputs from non-$POMC^{ARH}$ neurons. Consistently, it has been reported that $AgRP^{ARH}$ neurons innervate DA^{VTA} neurons[30]. Together, these data indicate that a subset of $POMC^{ARH}$ neurons project to DA^{VTA} neurons and non-DA^{VTA} neurons, and that DA^{VTA} neurons receive synaptic inputs from $POMC^{ARH}$ neurons and non-$POMC^{ARH}$ neurons.

Given the complex innervations from $POMC^{ARH}$ neurons to DA^{VTA} neurons and non-DA^{VTA} neurons, we further examined the neurotransmissions between $POMC^{ARH}$ neurons and several types of VTA neurons. To this end, we used an "upgraded" channelrhdopsin 2 (ChR2)-assisted circuit mapping (CRACM), which we named as WGA-CRACM. Briefly, we stereotaxically injected Cre-dependent AAV expressing ChR2-EYFP into the ARH of POMC-CreER/DAT-CreER/Rosa26-LSL-tdTOMATO mice to express ChR2 specifically in $POMC^{ARH}$ neurons and their fibers/terminals, which allows photostimulation (as shown Figure S2F). The same mice also received stereotaxic injections of Ad-FLEX-WGA-GFP, an anterograde trans-synaptic viral tracer[31], into the ARH. Ad-FLEX-WGA-GFP expressed GFP-tagged wheat germ agglutinin (WGA-GFP) in a Cre-dependent manner and therefore only $POMC^{ARH}$ neurons were filled with WGA-GFP. WGA-GFP is an anterograde trans-synaptic tracer, which labels the soma of downstream neurons that are immediately innervated by $POMC^{ARH}$ terminals[31]. Thus, GFP-labelled soma in the VTA were identified as the immediate targets of $POMC^{ARH}$ neurons. Note that these mice also express TOMATO in DA neurons due to the combination of DAT-CreER and Rosa26-LSL-tdTOMATO alleles. Therefore, GFP(+)TOMATO(+) neurons were identified as $POMC^{ARH}$-innervated DA^{VTA}

neurons, which account for about 43.66% GFP(+) neurons ($POMC^{ARH}$-innervated VTA neurons) and 31.40% TOMATO(+) neurons (DA^{VTA} neurons) (Figure S2G–I).

We then examined electrophysiological responses in $POMC^{ARH}$-innervated DA^{VTA} [GFP(+)TOMATO(+)] neurons (Figure 4A). Using a voltage clamp protocol, we detected excitatory post-synaptic current (EPSC) only in 9 out of 44 tested GFP(+)TOMATO(+) neurons evoked by blue light pulses (Figure 2B–C and S3A). The EPSC were mediated by glutamatergic neurotransmission as they were blocked by glutamate receptor inhibitors (CNQX and D-AP5); 4-AP and TTX failed to affect the EPSC, confirming a monosynaptic nature (Figure 2B–C). On the other hand, we failed to detect any light-evoked inhibitory post-synaptic current (IPSC) in all 20 tested GFP(+)TOMATO(+) neurons (Figure 2D and S3A). These results indicate that $POMC^{ARH}$ neurons provide minimal direct glutamatergic and none GABAergic inputs to DA^{VTA} neurons. Interestingly, under a current clamp mode, we found that blue light photostimulation caused rapid decreases in firing frequency and resting membrane potential in all 19 tested GFP(+)TOMATO(+) neurons (Figure 2E, J and K), indicating that $POMC^{ARH}$ neurons inhibit DA^{VTA} neurons. The lack of inhibitory IPSC observed at the $POMC^{ARH}\rightarrow DA^{VTA}$ synapse suggests that neuropeptides from $POMC^{ARH}$ neurons, e.g. α-MSH and β-endorphin, may mediate the inhibitory effects on DA^{VTA} neurons. Incubation of SHU9119, an antagonist of MC3R/MC4R, did not affect the inhibitory neurotransmission at the $POMC^{ARH}\rightarrow DA^{VTA}$ synapse (Figure 2F, J and K), indicating that α-MSH is not involved. Another neuropeptide, β-endorphin, could act upon one of 3 opioid receptors, namely δ-opioid receptor (DOR), κ-opioid receptor (KOR) and μ-opioid receptor (MOR). Thus, we tested effects of naltrindole (an antagonist of DOR), norbinaltorphimine (an antagonist of KOR), or cyprodime (an antagonist of MOR), respectively. While naltrindole and norbinaltorphimine did not affect the inhibitory neurotransmission at the $POMC^{ARH}\rightarrow DA^{VTA}$ synapse, incubation of cyprodime completely prevented the decreases in firing frequency and resting membrane potential in DA^{VTA} neurons evoked by photostimulation of $POMC^{ARH}$ projections (Figure 2G–K). Further, we collected 4 single neurons double-labelled by GFP and TOMATO ($POMC^{ARH}$-innervated DA^{VTA} neurons), and used RT-qPCR to detect expression of MC3R, MC4R and MOR mRNAs. None of these neurons expressed MC3R, and only one out of 4 neurons expressed MC4R mRNAs (Figure 2L). On the other hand, all 4 neurons expressed abundant MOR mRNAs (Figure 2L). Collectively, these results indicate that $POMC^{ARH}$ neurons inhibit DA^{VTA} neurons largely via MOR-mediated neurotransmission.

We then examined blue light-induced responses in $POMC^{ARH}$-innervated non-DA^{VTA} [GFP(+) only] neurons (Figure 3A). Under the voltage clamp mode, we observed light-evoked EPSC in 12 out of 42 tested neurons, which were blocked by CNQX and D-AP5 but were not affected by 4-AP and TTX (Figure 3B–C and S3B). On the other hand, we observed no light-evoked IPSC in all 21 tested neurons (Figure 3D and S3B). These results indicate that $POMC^{ARH}$ neurons provide minimal direct glutamatergic and no GABAergic inputs to these non-DA^{VTA} neurons, similar to their inputs to DA^{VTA} neurons. Under the current clamp mode, we found that blue light photostimulation caused rapid increases in firing frequency and resting membrane potential in 12 out of 14 tested GFP(+) neurons (Figure 3E), indicating that $POMC^{ARH}$ neurons activate these non-DA^{VTA} neurons. Interestingly, incubation of SHU9119, the antagonist of MC3R/MC4R, abolished the

excitation in these non-DA^{VTA} neurons caused by $POMC^{ARH}$ activation (Figure 3F–H), indicating that α-MSH mediates the excitatory neurotransmission at the majority of the $POMC^{ARH}$→non-DA^{VTA} synapse. To explore the chemical identity of these $POMC^{ARH}$-innervated non-DA^{VTA} neurons, we collected single neurons labelled by GFP only, and detected abundant vGAT mRNAs but minimal DAT mRNAs in these neurons (Figure 3I–J), indicating that these non-DA^{VTA} neurons are likely GABAergic neurons; as a positive control, abundant DAT mRNAs were detected in neurons labelled by both GFP and TOMATO (Figure 3J). In addition, the neurons labelled by GFP only expressed MC3R but no MC4R mRNAs, as well as abundant MOR mRNAs (Figure 3K). Further, we directly recorded from $GABA^{VTA}$ neurons (TOMATO-labelled VTA neurons in Vgat-IRES-Cre/Rosa26-LSL-tdTOMATO mice, Figure 3L), and found that a MC3R/MC4R agonist, MT-II, depolarized 10 out of 25 tested $GABA^{VTA}$ neurons in the presence of synaptic inhibitors (TTX, CNQX, D-AP5 and bicuculline); the other 15 $GABA^{VTA}$ neurons were not affected by MT-II (Figure 3M–N). Collectively, these data indicate that $POMC^{ARH}$ neurons release α-MSH to directly activate a portion of $GABA^{VTA}$ neurons via MC3R.

Finally, we examined blue light-induced responses in DA^{VTA} neurons that are not innervated by $POMC^{ARH}$ [TOMATO (+) only] neurons (Figure 4A). Under the voltage clamp mode, we did not observe any light-induced EPSC in all 23 tested neurons (Figure 4B and S3C); interestingly, we detected light-induced IPSC in 27 out of 42 tested TOMATO (+) neurons with an averaged latency of 101.30±8.15 ms (Figure 4C–D and S3C). Importantly, these light-evoked EPSC were inhibited by the $GABA_A$ receptor inhibitor, bicuculline, or by 4-AP and TTX (Figure 4C), suggesting an indirect neurotransmission mediated by GABAergic interneurons. Interestingly, in the presence of SHU9119 (the MC3R/MC4R antagonist), the light-evoked IPSC was only observed in 5 out of 21 tested neurons (P=0.0033 in $\chi 2$ test vs. the condition with no blockers; Figure 4C–D). Together, these results indicate that $POMC^{ARH}$ neurons can directly activate a portion of $GABA^{VTA}$ neurons through a MC3R-mediated mechanism, which in turn provide GABAergic inputs to a subset of DA^{VTA} neurons. Consistent with this indirect neurotransmission between $POMC^{ARH}$ neurons and DA^{VTA} neurons, we found, under the current clamp mode, that blue light photostimulation caused rapid decreases in firing frequency and resting membrane potential in 11 out of 14 tested TOMATO(+) neurons, effects that can be blocked by bicuculline, or by the MC3R/MC4R antagonist, SHU9119 (Figure 4E–I).

In summary, these results identify two parallel mechanisms by which $POMC^{ARH}$ neurons inhibit DA^{VTA} neurons. First, $POMC^{ARH}$ neurons directly innervate a subset of DA^{VTA} neurons and inhibit these neurons via a MOR-mediated mechanism. In addition, $POMC^{ARH}$ neurons indirectly inhibit another subset of DA^{VTA} neurons, largely through activating $GABA^{VTA}$ interneurons via a MC3R-mediated mechanism (Figure 4J). Notably, $POMC^{ARH}$ neurons also provide direct glutamatergic inputs to a small portion of DA^{VTA} and non-DA^{VTA} neurons. Since subsets of $POMC^{ARH}$ neurons are reported to be glutamatergic while the other subsets are GABAergic[32], we suggest that the VTA-projecting $POMC^{ARH}$ neurons are glutamatergic but not GABAergic.

Photoinhibition of the POMC^{ARH}→DA^{VTA} circuit partially ameliorates effects of chronic restraint stress

Given that POMC^{ARH} neurons inhibit DA^{VTA} neurons and that POMC^{ARH} neurons are activated while DA^{VTA} neurons are inhibited in RST mice, we sought to examine the functional relevance of the POMC^{ARH}→VTA circuit in the context of chronic restraint stress. To this end, we used optogenetic approach to selectively inhibit the POMC^{ARH}→VTA projections in RST mice. Briefly, we stereotaxically injected AAV-FLEX-eNpHR3.0-EYFP into the ARH of POMC-Cre mice to express eNpHR3.0 specifically in POMC^{ARH} neurons and their fibers/terminals; wild-type (WT) littermates received the same virus injections as controls (Figure 5A). These mice were also implanted with an optic fiber to target the VTA. After recovery, mice were subjected to the 1-hour/day RST paradigm for 14 days coupled to simultaneous 1-hour photoinhibition (Figure 5B). Compared to WT mice which decreased body weight during the 14-day RST period, POMC-Cre mice displayed significantly higher body weight (Figure 5C). Food intake of POMC-Cre mice were also significantly higher than that of WT mice at multiple time points (Figure 5D). These results indicate that inhibition of the POMC^{ARH}→VTA circuit increases body weight loss and feeding in mice exposed to chronic restraint stress.

We then examined the behavioral consequences in these mice after they completed the 14-day RST paradigm. Interestingly, POMC-Cre mice displayed significantly higher sucrose preference in the SPT, and lower immobility in FST and TST than WT mice (Figure 5E–G). These results indicate that inhibition of the POMC^{ARH}→VTA circuit ameliorates anhedonia and depression-like behaviors induced by chronic restraint stress.

Importantly, the same photoinhibition of the POMC^{ARH}→VTA projections in mice not subjected to the RST paradigm did not induce any significant changes in body weight, food intake or behaviors (Figure S4).

Discussion

In the current study, we demonstrated that chronic restraint stress leads to decreased DA^{VTA} neuron activity, associated with increased POMC^{ARH} neuron activity. We further found that POMC^{ARH} neurons inhibit DA^{VTA} neurons via direct or indirect mechanisms. In addition, selective inhibition of the POMC^{ARH}→VTA circuit partially increases body weight and feeding, and reduces anhedonia and depression-like behaviors in mice exposed to chronic restraint stress. Thus, our results provided evidence that the hyperactivity of the POMC^{ARH} neurons and their projections to the VTA contributes to the metabolic and mood dysregulations associated with chronic restraint stress.

The existence of a POMC^{ARH}→VTA circuit has been implicated by the Allen Brain Atlas (Experiment 263369222). Here we used the anterograde and retrograde tracing to further confirm that POMC^{ARH} neurons send projections to the VTA in the mouse brain. In addition, AgRP^{ARH} neurons also project to the VTA[30]. However, the detailed neurotransmissions between the hypothalamic melanocortin neurons and VTA neurons appear to be complex. On one hand, intra-VTA administration of α-MSH has been widely shown to increase DA release and turnover at efferent target sites, such as the nucleus

accumbens (NAc) and prefrontal cortex[33]. While α-MSH can act upon both melanocortin 3 and 4 receptors (MC3R and MC4R) in the brain[34], the stimulatory effects of α-MSH on DA turnover are thought to be mediated primarily by MC4R[35, 36]. Further, loss of AgRP signals (the endogenous antagonist of melanocortin receptors) results in enhanced DA^{VTA} neuron activity and elevated DA in basal forebrain[30]. On the other hand, it has been reported that abundant MC3R, but minimal MC4R, is expressed in the VTA[37]. Deletion of MC3R increases DA content in the VTA[37], suggesting the dominant effect of α-MSH on DA^{VTA} neurons may be inhibitory. Notably, $POMC^{ARH}$ neurons can also release β-endorphin which acts upon three different receptors, namely, KOR, DOR and MOR. All these receptors are located on presynaptic terminals of DA neurons to regulate DA release[38–40]. However, their effects on DA release are complicated and could be opposite depending on the time course of treatment[41] or on the subdivisions of projection targets[40]. In addition, MOR has been shown to be expressed by $GABA^{VTA}$ neurons, which receive inhibitory inputs from enkephalinergic neurons in the bed nucleus of stria terminalis (BNST) and inhibit DA^{VTA} neurons[42, 43]. Thus, the regulations on DA^{VTA} neurons are quite complex due to heterogeneous cell types within the VTA, to various neuromodulators originating from distinct upstream neurons, and to different receptor subtypes for these neuromodulators.

Here we focused on the $POMC^{ARH}$→VTA circuit, and used the WGA-CRACM approach which allowed us to examine 3 types of neurotransmissions with genetically identified pre-synaptic and post-synaptic nodes: $POMC^{ARH}$ neurons→DA^{VTA} neurons innervated by $POMC^{ARH}$ neurons, $POMC^{ARH}$ neurons →non-DA^{VTA} neurons innervated by $POMC^{ARH}$ neurons, and $POMC^{ARH}$ neurons→DA^{VTA} neurons not innervated by $POMC^{ARH}$ neurons. First, $POMC^{ARH}$ neurons directly synapse on and inhibit a subset of DA^{VTA} neurons, effects that can be completely blocked by the MOR antagonist. Consistently, modest levels of MOR mRNAs are present in this subset of DA^{VTA} neurons, while levels of MC3R and MC4R mRNAs are minimal. These results support a direct mechanism that some $POMC^{ARH}$ terminals in the VTA release β-endorphin which directly inhibits DA^{VTA} neurons through MOR-mediated neurotransmission.

On the other hand, $POMC^{ARH}$ neurons also directly synapse on and activate non-DA^{VTA} neurons. Importantly, these non-DA^{VTA} neurons innervated by $POMC^{ARH}$ neurons are largely GABAergic, and express modest levels of MC3R mRNAs but minimal MC4R mRNAs. We further showed that the α-MSH agonist directly inhibits a portion of identified $GABA^{VTA}$ neurons, similarly as reported by others[44]. Notably, these non-DA^{VTA} neurons innervated by $POMC^{ARH}$ neurons also express abundant MOR mRNAs, although the functional relevance of MOR in this subset of neurons was not directly tested in the current study.

Interestingly, we found that $POMC^{ARH}$ neurons can also inhibit DA^{VTA} neurons that are not direct synaptic targets of $POMC^{ARH}$ neurons. Since these inhibitory effects (both IPSC and decreased firing and resting membrane potential) are blunted by the $GABA_A$ receptor inhibitor or by the α-MSH antagonist, we postulate an indirect mechanism that $POMC^{ARH}$ neurons activate $GABA^{VTA}$ neurons, which in turn inhibit a subset of DA^{VTA} neurons. Consistent with this indirect mechanism, earlier studies indicate that $GABA^{VTA}$ interneurons provide local GABAergic inhibitory inputs to adjacent DA^{VTA} neurons[42, 45, 46]. Together,

our data demonstrate that $POMC^{ARH}$ neurons provide an inhibitory tone to DA^{VTA} neurons through both direct and indirect neurotransmissions. Notably, a portion of $POMC^{ARH}$ neurons express molecular machinery for synthesis and secretion of glutamate and GABA[32, 47]. However, we only observed glutamate-mediated EPSC in a small portion of $POMC^{ARH}$-innervated VTA neurons and no GABA-mediated IPSC was observed. We suggest that only a modest subset of glutamatergic $POMC^{ARH}$ neurons and minimal GABAergic $POMC^{ARH}$ neurons project to the VTA, while the majority of VTA-projecting $POMC^{ARH}$ neurons use α-MSH or β-endorphin as the dominant neuro-signal. It is worth mentioning that $POMC^{ARH}$ neurons have modest projections to the NAc[48], which may regulate DA release through their actions on the DA^{VTA}-originated terminals within the NAc. A limitation of our WGA-CRACM approach is that it can only assess the neurotransmission at the cell bodies of VTA neurons, but could not measure potential inputs of $POMC^{ARH}$ neurons to neural terminals that originate from the VTA.

Restraint stress causes increased activity of $POMC^{ARH}$ neurons but decreased activity of DA^{VTA} neurons. Given that $POMC^{ARH}$ neurons inhibit DA^{VTA} neurons, we suggest a model that restraint stress results in hyperactivity of $POMC^{ARH}$ neurons, which in turn inhibit DA^{VTA} neurons. Further supporting the functional relevance of the $POMC^{ARH}\rightarrow VTA$ circuit, the optogenetic study demonstrates that inhibition of the $POMC^{ARH}\rightarrow VTA$ projections ameliorates anhedonia and depression-like behaviors induced by chronic restraint stress. Since receptors for β-endorphin and α-MSH both contribute to the $POMC^{ARH}\rightarrow VTA$ circuit, we speculate that these receptors within the VTA may be involved in the development of anhedonia and depression-like in animals exposed to chronic restraint stress. While KOR does not seem to regulate anhedonia and depression-like behaviors, genetic deficiency in either DOR or MOR alters animal's depression level with opposite effects[49]. For example, DOR knockout mice have increased depression[49], whereas MOR knockout mice show decreased depression-like behaviors[50]. In particular, chronic stress (e.g. social defeat) robustly enhances MOR levels in the VTA[51, 52]; selective knockdown of MOR in rat VTA prevents social avoidance induced by social stress exposure[53]. Together with our observations that the inhibitory effects of $POMC^{ARH}$ neurons on DA^{VTA} neurons are partially mediated by a direct MOR-dependent neurotransmission, these findings support a possibility that MOR in the VTA contributes to the development of anhedonia and depression-like behavior during chronic restraint stress. Alternatively, α-MSH-mediated activation of $GABA^{VTA}$ neurons may provide an indirect mechanism to inhibit DA^{VTA} neurons, which raises the possibility that α-MSH signals within these $GABA^{VTA}$ neurons may be partly responsible for anhedonia and depression-like behaviors triggered by chronic restraint stress. Consistently, global deletion of MC3R results in increased dopamine bioavailability in the VTA in mice[37]. Further, administration of MTII, the MC3R/MC4R agonist, into the VTA decreases food intake and sucrose preference in rats, while the MC3R/MC4R antagonist (SHU9119) causes opposite effects[54–56]. However, global deletion of MC3R leads to decreased sucrose preference only in female mice but not in male mice[37], phenotypes that may have been confounded by loss of MC3R in all types of cells since early development. Thus, the specific roles of MC3R in different subgroups of VTA neurons during adulthood warrant further investigations.

We also found that chronic photoinhibition of the POMC^{ARH}→VTA projections increases food intake and body weight in RST mice. Consistently, chronic chemogenetic stimulation of POMC^{ARH} neurons decreases food intake in mice, although acute stimulation of these neurons fails to alter feeding behavior[57]. However, most of anorexigenic effects of POMC^{ARH} neurons are thought to be mediated by MC4R expressed in the paraventricular nucleus of hypothalamus (PVH)[58]. Our results suggest that the POMC^{ARH}→VTA circuit is an alternative pathway by which POMC^{ARH} neurons can reduce food intake at least in the context of chronic stress. Supporting a feeding-suppressing effect of α-MSH in the VTA, it has been reported that injections of MT-II into the VTA decrease food intake, while intra-VTA injections of SHU9119 increase feeding[55, 56]. Interestingly, knockdown of MOR in the VTA prevents body weight loss induced by social defeat[53]. Thus, the MOR-mediated neurotransmission we observed in the VTA may also contribute to hypophagia and body weight loss during chronic restraint stress. This possibility remains to be investigated.

Neurocircuits regulating mood and feeding behavior are at least partly overlapping, which provides important defensive mechanisms for animals to coordinate internal states (e.g. energy balance and mood) with complex external environment (e.g. food availability, danger and stress)[59]. In particular, hunger activates AgRP^{ARH} neurons, which reduce anxiety[60, 61], fear[62] and pain[63], and ultimately facilitate food-seeking behavior to ensure survival. Here we showed that alternations of the POMC^{ARH}→VTA circuit during stress result in abnormal feeding and mood, which is another example that feeding behavior, depression-like behavior and anhedonia are not separate entities, but rather they may influence each other reciprocally. POMC^{ARH} neurons, via their projections to the reward circuitry, provide one neurobiological basis to coordinate feeding and mood regulations in response to chronic stress. Consistent with our findings in mice, the neural activities of the VTA in human brains are correlated with craving behavior[64]. Further, humans with depression often display reduced neural connectivity from the VTA to its downstream targets, including the striatum[65] and the dorsal anterior cingulate cortex[66]. Interestingly, mutations in the gene encoding MOR have been associated with human depression[67], supporting the possibility that POMC-originated signals, e.g. β-endorphin, contribute to development of depression, and that the POMC^{ARH}→VTA circuit may exist in human brains. Nevertheless, further investigations are needed to confirm such POMC^{ARH}→VTA circuit in human brains and to explore its role in human depression.

Methods

Mice

Multiple lines of transgenic mice were used in the current study. For electrophysiological studies, we crossed Rosa26-LSL-tdTOMATO allele[68] (obtained from Jackson Laboratory, #007905) onto DAT-CreER (Jackson Laboratory, #016583), POMC-CreER[69], AgRP-IRES-Cre mice[70] or Vgat-IRES-Cre mice[71] (Jackson Laboratory, #028862), respectively. These crosses generated mice with TOMATO selectively expressed in DA, POMC (after tamoxifen inductions), AgRP or GABAergic neurons. We crossed C57Bl6j mice with POMC-Cre mice[72] to generate POMC-Cre and wild-type littermates. We crossed POMC-CreER, DAT-CreER and Rosa26-LSL-tdTOMATO mice to generate POMC-CreER/DAT-CreER/Rosa26-

LSL-tdTOMATO mice. All the breeders have been backcrossed to C57Bl6j background for more than 12 generations. In addition, some C57Bl6j mice were purchased from the mouse facility of Baylor College of Medicine. Mice were housed in a temperature-controlled environment in groups of two to five at 22°C-24°C using a 12 hr light/12 hr dark cycle. The mice were fed standard chow (6.5% fat, #2920, Harlan-Teklad, Madison, WI) *ad libitum*. Water was provided *ad libitum*.

RST Protocol

The experiments were performed after the animals had been habituated to the experimental environment for 1 week. In the study described in Figure 1, male C57Bl6j mice (3 months of age) were divided into two weight-matched groups: control group (CON) and restraint stress group (RST). The RST mice were exposed daily for 14 days to 1-hour restraint (9:30–10:30am) in rodent restraint plastic bags (Triangle-shaped Restraints 1800c #89066–356, VWR AIMS$_{TM}$) with holes that permit the mice breathing but restrict the movement of the limbs; the CONT mice were left intact. In the study described in Figure 7, male WT and POMC-Cre littermates were anesthetized with isoflurane and received stereotaxic injections of the silencer of AAV-hSyn-eNpHR3.0-EYFP virus (University of North Carolina Gene Therapy Center, Chapel Hill, NC) into both sides of the ARH (250 nL/site, −1.7 mm posterior, ±0.25 mm lateral and −5.8 mm ventral to the Bregma, based on Franklin & Paxinos Mouse Brain Atlas). During the same surgery, an optic fiber was implanted to target the VTA (unilateral, −3 mm posterior, 0.5 mm lateral and −4.3 mm ventral to the Bregma). After a 4-week recovery, these mice (4 months of age) were subjected to the 14-day RST protocol as described above, and during the daily 1-hour restraint, the mice also received yellow light stimulation (589 nm, 10 ms/pulse, 3 pulses per 1 s for 1 hour; MGL-FN-589, CNI LASER). A small hole was made in the restraint plastic bag to allow insertion of the optic fiber. After being restrained, the mice were returned to their home cages and given food and water *ad libitum*. The food intake and body weight of the mice were monitored daily.

Behavioral tests

All behavioral tests were performed during the afternoon in a dedicated sound-proof behavioral facility by experimenters blind to treatment and genotype information. Mice were brought to the procedure room 1 hour before the start of each behavioral test and remained in the same room throughout the test. At all times, sound was masked with 60–65 Db white noise.

Mice were allowed to rest for one day after the completion of the 14-day RST protocol. Then, sucrose preference tests were performed on day 16. A bottle with tap water and another bottle with 2% sucrose solution were given to mice. The mice had been trained (given a free choice between two bottles) for 1 hour every day (12:30pm-1:30pm, on day 8 to day 14) to avoid neophobia. To prevent a possible effect of behavior, the left/right location of the bottles was switched every day. The sucrose preference was calculated as the ratio of consumed sucrose solution to consumed water.

Forced swim tests were performed on day 17. In brief, mice were placed in a glass cylinder (height: 50 cm, diameter: 20 cm) containing water at 23–25 °C and depth of 14 cm, such that mice could neither escape nor touch the bottom. Mice were forced to swim for 6 min. Mice were acclimated for the first 1 min and immobility time was measured for the last 5 min.

Tail suspension tests were performed on day 18. Mice were suspended individually by their tails from a metal rod fixed 30 cm above the surface of a table. The tip of the tail was fixed using adhesive tape (the distance from tip of tail was 2 cm). The subject mouse was suspended by the tail for 6 min. Mice were acclimated for the first 1 min and immobility time was measured for the last 5 min.

All mice that received stereotaxic injections were perfused with 10% formalin after the completion of the behavioral tests. Brain sections were collected, and expression of EYFP was checked in the ARH. Only those with expression of EYFP exclusively in the ARH were included in data analyses. All behavioral analyses were performed by experimenters who were blinded with the treatment groups.

Electrophysiology

To examine the activities of DA^{VTA}, $POMC^{ARH}$ and $AgRP^{ARH}$ neurons in RST mice, DAT-CreER/Rosa26-LSL-tdTOMATO mice (after tamoxifen induction), POMC-CreER/Rosa26-LSL-tdTOMATO mice (after tamoxifen induction), and AgRP-IRES-Cre/Rosa26-LSL-tdTOMATO mice were subjected to RST or CON protocol as described above, for 4 days. Immediately after the last session of restraint (or control), these mice were deeply anesthetized with isoflurane and perfused with a modified ice-cold sucrose-based cutting solution (pH 7.3) containing 10 mM NaCl, 25 mM $NaHCO_3$, 195 mM Sucrose, 10 mM Glucose, 2.5 mM KCl, 1.25 mM NaH_2PO_4, 2 mM Na-Pyruvate, 0.5 mM $CaCl_2$, and 7 mM $MgCl_2$, bubbled continuously with 95% O_2 and 5% CO_2 (Ren et al., 2012). The mice were then decapitated, and the entire brain was removed and immediately submerged in the cutting solution. Slices (250 μm) were cut with a Microm HM 650V vibratome (Thermo Scientific). Coronal brain slices containing the VTA or ARH were obtained for each animal. The slices were recovered for 1 h at 34°C and then maintained at room temperature in artificial cerebrospinal fluid (aCSF, pH 7.3) containing 126 mM NaCl, 2.5 mM KCl, 2.4 mM $CaCl_2$, 1.2 mM NaH_2PO_4, 1.2 mM $MgCl_2$, 5.0 mM glucose, and 21.4 mM $NaHCO_3$) saturated with 95% O_2 and 5% CO_2 before recording.

Slices were transferred to a recording chamber and allowed to equilibrate for at least 10 min before recording. The slices were superfused at 34°C in oxygenated aCSF at a flow rate of 1.8–2 ml/min. TOMATO-labeled neurons were visualized using epifluorescence and IR-DIC imaging on an upright microscope (Eclipse FN-1, Nikon) equipped with a movable stage (MP-285, Sutter Instrument). Patch pipettes with resistances of 3–5 MΩ were filled with intracellular solution (pH 7.3) containing 128 mM K-Gluconate, 10 mM KCl, 10 mM HEPES, 0.1 mM EGTA, 2 mM $MgCl_2$, 0.05 mM Na-GTP and 0.05 mM Mg-ATP. Recordings were made using a MultiClamp 700B amplifier (Axon Instrument), sampled using Digidata 1440A and analyzed offline with pClamp 10.3 software (Axon Instruments). Series resistance was monitored during the recording, and the values were generally <10 MΩ and were not compensated. The liquid junction potential was +12.5 mV, and was corrected

after the experiment. Data were excluded if the series resistance increased dramatically during the experiment or without overshoot for action potential. Currents were amplified, filtered at 1 kHz, and digitized at 20 kHz. Current clamp was engaged to test neural firing frequency and resting membrane potential[73]. The values were averaged within 2-min bin. After-hyperpolarization potential (AHP) of DA^{VTA} neurons was calculated by substracting the most negative membrane potential right after the decay of each action potential to the onset membrane potential before the action potential. The AHP value from each neuron was averaged by 3 different single AHP in the same trace. To analyze these parameters (firing frequency, resting membrane potential and AHP), we first treated each neuron as an independent biological sample; in addition, we also calculated the average of all neurons from the same mouse and treated each mouse as an independent biological sample. Both analyses were presented in the figures.

To examine effects of MT-II on $GABA^{VTA}$ neurons, the VTA-containing brain slices were prepared from 8-week old Vgat-IRES-Cre/Rosa26-LSL-tdTOMATO mice, as described above. The brain slices were incubated with the cocktail inhibitors containing 1μM TTX, 30μM CNQX, 30 μM D-AP5, 50 μM bicuculline in order to block most of the synaptic inputs on $GABA^{VTA}$ neurons. 300 nM MT-II was perfused to treat the $GABA^{VTA}$ neurons in the presence of the cocktail blockers. The change of resting membrane potential after MT-II treatment was recorded.

After recording of each neuron, a lucifer yellow dye was injected into the recorded neuron via the pipette. Slices were fixed with 4% formalin in PBS at 4°C overnight and then subjected to post hoc identification of the anatomical location of the recorded neurons within the ARH or the VTA.

Neurotracing

To determine whether $POMC^{ARH}$ neurons project to the VTA, twelve-week old POMC-Cre mice were anesthetized by isoflurane and received stereotaxic injections of Cre-dependent AAV expressing Synaptophysin-GFP (AAV-FLEX-Synaptophysin-GFP) into the ARH (200 nl). Four weeks after injections, mice were perfused with 10% formalin, and brain sections were cut at 25 μm (5 series). These brain sections were subjected to immunofluorescence staining for TH with rabbit anti-Tyrosine hydroxylase antibody (1:500, AB152, Millipore, Temecula, CA) overnight, followed by the goat anti-rabbit AlexaFluor 405 (1:500, A31556, Invitrogen) for 1.5 h. Slides were cover-slipped and analyzed using a Leica DM5500 fluorescence microscope with OptiGrid structured illumination configuration.

To determine whether DA^{VTA} neurons receive projections from $POMC^{ARH}$ neurons, twelve-week old DAT-CreER mice were anesthetized by isoflurane and received stereotaxic injections of AAV8-EF1a-FLEX-GTB (1.16E+12 GC/ml, Salk Institute for Biological Studies) in the VTA (200nl). These mice were recovered for 4 days and received tamoxifen (0.2mg/g, i.p) injection to induce the expression of Cre in DA neurons. One week after tamoxifen injection, the mice received the second stereotaxic injections of EnvA G-deleted Rabies-mCherry (1.08E+9 TU/ml, Salk Institute for Biological Studies) virus in the VTA (200nl). Four weeks after, the mice were perfused as above. Brain sections were then subjected to immunofluorescent staining for β-endorphin. Briefly, sections were incubated

with primary rabbit anti-β-endorphin antibody (1:10000, H-022–33, Phoenix Peptide) overnight, followed by the donkey anti-rabbit AlexaFluor 488 (1:500, A21206, Invitrogen) for 1.5 h. The sections were mounted on glass slides and fluorescence images were analyzed using a Leica DM5500 fluorescence microscope with OptiGrid structured illumination configuration. The DA^{VTA} neurons infected with both AAV8-FLEX-GTB and Env-dG-Rabies and the retrograde traced neurons were labeled by mCherry (red), and POMC neurons were labeled by β-endorphin (green).

WGA-CRACM

We performed the channelrhodopsin-2 (ChR2)-assisted circuit mapping (CRACM), similarly as described by others[74, 75], in order to examine the neurotransmissions between $POMC^{ARH}$ neurons and VTA neurons. Briefly, 12-week old POMC-CreER/DAT-CreER/Rosa26-LSL-tdTOMATO mice were anesthetized by isoflurane and received stereotaxic injections of Ad-FLEX-WGA-GFP (100 nl/site) and AAV-EF1α-DIO hChR2(H134R)-EYFP (100 nl/site) into the ARH. Tamoxifen (0.2 mg/g, i.p.) was injected into these mice to induce POMC-CreER and DAT-CreER. After a 4-week recovery, mice were sacrificed and unfixed brain slices (containing both the ARH and VTA, 120 μm in thickness) were prepared from these mice. These brain slices were subjected to fluorescent microscopy to visualize and quantify GFP(+), TOMATO(+) and GFP(+)/TOMATO(+) neural soma in the VTA. Notably, EYFP expressed by the AAV-EF1α-DIO hChR2(H134R)-EYFP shares overlapping spectra with GFP. However, EYFP will only label the fibers and terminals in the VTA but will not cross the synapse to label the soma of downstream neurons. Thus, the GFP-labelled soma within the VTA must be filled by WGA-GFP fusion proteins. About 150–160 neural soma were counted from each mouse and 3 mice were included. These brain slices were also used to perform electrophysiological recordings, as described below.

Under the voltage clamp mode, light-evoked EPSCs or IPSCs were recorded in GFP(+), TOMATO(+) or GFP(+)/TOMATO(+) VTA neurons in brain slices in response to 473 nM laser blue light (10 Hz, 10 ms pulse, 0.2 mW; MBL-FN-473, CNI LASER). The light sThe light-evoked EPSCs were recorded in whole-cell voltage-clamp mode, by holding the membrane potential at Vh = −60 mV. The pipette solution containing: 125 mM $CsCH_3SO_3$; 10 mM CsCl; 5 mM NaCl; 2 mM $MgCl_2$; 1 mM EGTA; 10 mM HEPES; 5 mM (Mg)ATP; 0.3 mM $(Na)_2GTP$ (pH 7.3 with NaOH). The light evoked IPSCs were recorded in whole-cell voltage-clamp mode, by holding the membrane potential at Vh = −70 mV. The CsCl-based pipette solution containing of: 140mM CsCl, 10mM HEPES, 5mM $MgCl_2$, 1mM BAPTA, 5mM (Mg)ATP, and 0.3mM $(Na)_2GTP$ (pH 7.30 adjusted with NaOH; 295 mOsm kg^{-1}). TTX (1μM) and 4-AP (400 μM) were added to the aCSF in order to confirm the response was monosynaptic responses. EPSCs were recorded when 50 μM bicuculline was applied in the bath solution; after evoked EPSC was detected, 30 μM D-AP5 and 30 μM CNQX were used to confirm the current was mediated by glutamate receptors. IPSCs were recorded when 30 μM D-AP5 and 30 μM CNQX were applied in the bath solution; after evoked IPSC was detected, 50 μM bicuculline was used to confirm the current was mediated by $GABA_A$ receptor. In some experiments, 50 μM SHU9119 was treated after evoked IPSC was detected. Under the current clamp mode, 30 μM D-AP5, 30 μM CNQX and 50 μM bicuculline were applied in the bath solution to block the glutamate and GABA inputs;

action potential firing rate and resting membrane potential were recorded in response to 473 nM blue light (10 Hz, 10 ms pulse, 0.2 mW) in the absence or presence of various blockers, such as 50 μM SHU9119[76], 100 μM naltrindole[77], 100 μM norbinaltorphimine[78], 200 μM cyprodime[79].

Single neuron RT-PCR

To determine the neurochemical identify of $POMC^{ARH}$-innervated VTA neurons in the WGA-CRACM study, we manually picked up GFP(+) neurons and GFP(+)/TOMATO(+) neurons, and suspended in PBS buffer. Briefly, the mice brain was removed and immediately submerged in ice-cold sucrose-based cutting solution (adjusted to pH 7.3) containing (in mM) 10 NaCl, 25 NaHCO3, 195 Sucrose, 5 Glucose, 2.5 KCl, 1.25 NaH_2PO_4, 2 Na pyruvate, 0.5 $CaCl_2$, 7 $MgCl_2$ bubbled continuously with 95% O_2 and 5% CO_2. The slices (250 μm) were cut with a Microm HM 650V vibratome (Thermo Scientific and recovered for 1 h at 34°C and then maintained at room temperature in artificial cerebrospinal fluid (aCSF, pH 7.3) containing 126 mM NaCl, 2.5 mM KCl, 2.4 mM $CaCl_2$, 1.2 mM NaH_2PO_4, 1.2 mM $MgCl_2$, 11.1 mM glucose, and 21.4 mM $NaHCO_3$ saturated with 95% O_2 and 5% CO_2 before recording. Slices were transferred to a chamber, and GFP(+) neurons and GFP(+)/TOMATO(+) neurons were visualized using epifluorescence and IR-DIC imaging on an upright microscope equipped with a moveable stage (MP-285, Sutter Instrument). Single neurons were manually picked up by the pipette and 2 neurons were combined as a sample for RNA extraction and reverse transcription using the Ambion Single-Cell-to-CT Kit (Ambion, Life Technologies) according to the manufacturer's instruction. Briefly, 30 μl Single Cell Lysis solutions with DNase I was added to each sample, and the supernatant after centrifuge were used for cDNA synthesis (25°C for 10 min, 42°C for 60 min, and 85°C for 5 min). The cDNA samples were amplified on a CFX384 Real-Time System (Bio-Rad) using SsoADV SYBR Green Supermix (Bio-Rad). Results were normalized against the expression of house-keeping gene (β-actin). Primer sequences for β-actin, DAT and Vgat and DAT: β-actin forward, ATGGAGGGGAATACAGCCC; β-actin reverse, TTCTTTGCAGCTCCTTCGTT; DAT forward, TGATGCACATAGCAGCAACTC; DAT reverse, AGGTCATCAATGCCACGACT; Vgat forward, CGACAAACCCAAGATCACGG; Vgat reverse, AGGATGGCGTAGGGTAGGC; MC3R forward, TCCGATGCTGCCTAACCTCT; MC3R reverse, GGATGTTTTCCATCAGACTGACG; MC4R forward, GGTCGGAAACCATCGTCATT; MC4R reverse, AAAGCAGGCTGCAAATGGAT; MOR forward, CCAGGGAACATCAGCGACTG; MOR reverse, GTTGCCATCAACGTGGGAC.

Statistics

The minimal sample size was pre-determined by the nature of experiments. For most of physiological readouts (body weight, food intake, etc.), 5–7 mice per group were included. For histology studies, 3 mice were included in each group. For electrophysiological studies, at least 10 neurons in each genotype or condition were included. The data are presented as mean ± SEM. Statistical analyses were performed using GraphPad Prism to evaluate normal distribution and variations within and among groups. Methods of statistical analyses were

chosen based on the design of each experiment and are indicated in figure legends. $P<0.05$ was considered to be statistically significant.

Study approval

Care of all animals and procedures were approved by the Baylor College of Medicine Institutional Animal Care and Use Committee.

Supplementary Material

Refer to Web version on PubMed Central for supplementary material.

Acknowledgements:

This work was supported by grants from the NIH (K99DK107008 to P.X.; R01DK111436, R01ES027544, R21CA215591 to Z.S.), USDA/CRIS (6250–51000-059–04S to Y.X.), American Diabetes Association (1–17-PDF-138 to Y.H), American Heart Association awards (17GRNT32960003 to Y.X., 16GRNT30970064 to Z.S., and 16POST27260254 to C. W.), National Natural Science Foundation of China (81400886 to N.Q.), Hubei Province health and family planning scientific research project (WJ2015Q033 to N.Q.) and Population and Family Planning Commission of Wuhan (WX14B34 to N.Q.). The author also appreciated support by award and fellowships from Wuhan Young & Middle-Aged Talents, Health and Family Planning Commission of Wuhan Municipality and China Scholarship Council (File NO.201608420019 to N.Q.).

Reference

1. McEwen BS, Morrison JH. The brain on stress: vulnerability and plasticity of the prefrontal cortex over the life course. Neuron 2013; 79(1): 16–29. [PubMed: 23849196]
2. Krahn DD, Gosnell BA, Majchrzak MJ. The anorectic effects of CRH and restraint stress decrease with repeated exposures. Biol Psychiatry 1990; 27(10): 1094–1102. [PubMed: 2340320]
3. Jeong JY, Lee DH, Kang SS. Effects of chronic restraint stress on body weight, food intake, and hypothalamic gene expressions in mice. Endocrinol Metab (Seoul) 2013; 28(4): 288–296. [PubMed: 24396694]
4. Chuang JC, Krishnan V, Yu HG, Mason B, Cui H, Wilkinson MB et al. A beta3-adrenergic-leptin-melanocortin circuit regulates behavioral and metabolic changes induced by chronic stress. Biol Psychiatry 2010; 67(11): 1075–1082. [PubMed: 20060958]
5. Holly EN, Miczek KA. Ventral tegmental area dopamine revisited: effects of acute and repeated stress. Psychopharmacology (Berl) 2016; 233(2): 163–186. [PubMed: 26676983]
6. Barker DJ, Root DH, Zhang S, Morales M. Multiplexed neurochemical signaling by neurons of the ventral tegmental area. J Chem Neuroanat 2016; 73: 33–42. [PubMed: 26763116]
7. Morales M, Margolis EB. Ventral tegmental area: cellular heterogeneity, connectivity and behaviour. Nat Rev Neurosci 2017; 18(2): 73–85. [PubMed: 28053327]
8. Yamaguchi T, Sheen W, Morales M. Glutamatergic neurons are present in the rat ventral tegmental area. Eur J Neurosci 2007; 25(1): 106–118. [PubMed: 17241272]
9. Willner P. Dopamine and depression: a review of recent evidence. I. Empirical studies. Brain Res 1983; 287(3): 211–224. [PubMed: 6140979]
10. Chiodo LA, Antelman SM. Electroconvulsive shock: progressive dopamine autoreceptor subsensitivity independent of repeated treatment. Science 1980; 210(4471): 799–801. [PubMed: 6254148]
11. Tye KM, Mirzabekov JJ, Warden MR, Ferenczi EA, Tsai HC, Finkelstein J et al. Dopamine neurons modulate neural encoding and expression of depression-related behaviour. Nature 2013; 493(7433): 537–541. [PubMed: 23235822]
12. Friedman AK, Walsh JJ, Juarez B, Ku SM, Chaudhury D, Wang J et al. Enhancing depression mechanisms in midbrain dopamine neurons achieves homeostatic resilience. Science 2014; 344(6181): 313–319. [PubMed: 24744379]

13. Sidor MM, Spencer SM, Dzirasa K, Parekh PK, Tye KM, Warden MR et al. Daytime spikes in dopaminergic activity drive rapid mood-cycling in mice. Mol Psychiatry 2015; 20(11): 1406–1419. [PubMed: 25560763]
14. Liu J, Perez SM, Zhang W, Lodge DJ, Lu XY. Selective deletion of the leptin receptor in dopamine neurons produces anxiogenic-like behavior and increases dopaminergic activity in amygdala. Mol Psychiatry 2011; 16(10): 1024–1038. [PubMed: 21483433]
15. Son DH, Doan KV, Yang DJ, Sun JS, Kim SK, Kang N et al. FoxO1 regulates leptin-induced mood behavior by targeting tyrosine hydroxylase. Metabolism 2019; 91: 43–52. [PubMed: 30500562]
16. Liu W, Liu J, Xia J, Xue X, Wang H, Qi Z et al. Leptin receptor knockout-induced depression-like behaviors and attenuated antidepressant effects of exercise are associated with STAT3/SOCS3 signaling. Brain Behav Immun 2017; 61: 297–305. [PubMed: 28069387]
17. Zhou QY, Palmiter RD. Dopamine-deficient mice are severely hypoactive, adipsic, and aphagic. Cell 1995; 83(7): 1197–1209. [PubMed: 8548806]
18. Szczypka MS, Rainey MA, Kim DS, Alaynick WA, Marck BT, Matsumoto AM et al. Feeding behavior in dopamine-deficient mice. Proc Natl Acad Sci U S A 1999; 96(21): 12138–12143. [PubMed: 10518589]
19. Boekhoudt L, Roelofs TJM, de Jong JW, de Leeuw AE, Luijendijk MCM, Wolterink-Donselaar IG et al. Does activation of midbrain dopamine neurons promote or reduce feeding? Int J Obes (Lond) 2017; 41(7): 1131–1140. [PubMed: 28321131]
20. Elmquist JK, Elias CF, Saper CB. From lesions to leptin: hypothalamic control of food intake and body weight. Neuron 1999; 22(2): 221–232. [PubMed: 10069329]
21. Cone RD. Anatomy and regulation of the central melanocortin system. Nat Neurosci 2005; 8(5): 571–578. [PubMed: 15856065]
22. Williams DL, Schwartz MW. The melanocortin system as a central integrator of direct and indirect controls of food intake. Am J Physiol Regul Integr Comp Physiol 2005; 289(1): R2–3. [PubMed: 15956761]
23. Cone RD. The Central Melanocortin System and Energy Homeostasis. Trends Endocrinol Metab 1999; 10(6): 211–216. [PubMed: 10407394]
24. Huszar D, Lynch CA, Fairchild-Huntress V, Dunmore JH, Fang Q, Berkemeier LR et al. Targeted disruption of the melanocortin-4 receptor results in obesity in mice. Cell 1997; 88(1): 131–141. [PubMed: 9019399]
25. Koch M, Varela L, Kim JG, Kim JD, Hernandez-Nuno F, Simonds SE et al. Hypothalamic POMC neurons promote cannabinoid-induced feeding. Nature 2015; 519(7541): 45–50. [PubMed: 25707796]
26. Appleyard SM, Hayward M, Young JI, Butler AA, Cone RD, Rubinstein M et al. A role for the endogenous opioid beta-endorphin in energy homeostasis. Endocrinology 2003; 144(5): 1753–1760. [PubMed: 12697680]
27. Yang Y, Atasoy D, Su HH, Sternson SM. Hunger states switch a flip-flop memory circuit via a synaptic AMPK-dependent positive feedback loop. Cell 2011; 146(6): 992–1003. [PubMed: 21925320]
28. Grandison L, Guidotti A. Stimulation of food intake by muscimol and beta endorphin. Neuropharmacology 1977; 16(7–8): 533–536. [PubMed: 917261]
29. Seo JS, Wei J, Qin L, Kim Y, Yan Z, Greengard P. Cellular and molecular basis for stress-induced depression. Mol Psychiatry 2017; 22(10): 1440–1447. [PubMed: 27457815]
30. Dietrich MO, Bober J, Ferreira JG, Tellez LA, Mineur YS, Souza DO et al. AgRP neurons regulate development of dopamine neuronal plasticity and nonfood-associated behaviors. Nat Neurosci 2012; 15(8): 1108–1110. [PubMed: 22729177]
31. Leinninger GM, Opland DM, Jo YH, Faouzi M, Christensen L, Cappellucci LA et al. Leptin action via neurotensin neurons controls orexin, the mesolimbic dopamine system and energy balance. Cell Metab 2011; 14(3): 313–323. [PubMed: 21907138]
32. Wittmann G, Hrabovszky E, Lechan RM. Distinct glutamatergic and GABAergic subsets of hypothalamic pro-opiomelanocortin neurons revealed by in situ hybridization in male rats and mice. J Comp Neurol 2013; 521(14): 3287–3302. [PubMed: 23640796]

33. Roseberry AG, Stuhrman K, Dunigan AI. Regulation of the mesocorticolimbic and mesostriatal dopamine systems by alpha-melanocyte stimulating hormone and agouti-related protein. Neurosci Biobehav Rev 2015; 56: 15–25. [PubMed: 26116876]

34. Anderson EJ, Cakir I, Carrington SJ, Cone RD, Ghamari-Langroudi M, Gillyard T et al. 60 YEARS OF POMC: Regulation of feeding and energy homeostasis by alpha-MSH. J Mol Endocrinol 2016; 56(4): T157–174. [PubMed: 26939593]

35. Lindblom J, Opmane B, Mutulis F, Mutule I, Petrovska R, Klusa V et al. The MC4 receptor mediates alpha-MSH induced release of nucleus accumbens dopamine. Neuroreport 2001; 12(10): 2155–2158. [PubMed: 11447325]

36. Yang SC, Shieh KR. Differential effects of melanin concentrating hormone on the central dopaminergic neurons induced by the cocaine- and amphetamine-regulated transcript peptide. J Neurochem 2005; 92(3): 637–646. [PubMed: 15659233]

37. Lippert RN, Ellacott KL, Cone RD. Gender-specific roles for the melanocortin-3 receptor in the regulation of the mesolimbic dopamine system in mice. Endocrinology 2014; 155(5): 1718–1727. [PubMed: 24605830]

38. Svingos AL, Chavkin C, Colago EE, Pickel VM. Major coexpression of kappa-opioid receptors and the dopamine transporter in nucleus accumbens axonal profiles. Synapse 2001; 42(3): 185–192. [PubMed: 11746715]

39. Svingos AL, Clarke CL, Pickel VM. Localization of the delta-opioid receptor and dopamine transporter in the nucleus accumbens shell: implications for opiate and psychostimulant cross-sensitization. Synapse 1999; 34(1): 1–10. [PubMed: 10459166]

40. Hipolito L, Sanchez-Catalan MJ, Zanolini I, Polache A, Granero L. Shell/core differences in mu- and delta-opioid receptor modulation of dopamine efflux in nucleus accumbens. Neuropharmacology 2008; 55(2): 183–189. [PubMed: 18582908]

41. Chartoff EH, Ebner SR, Sparrow A, Potter D, Baker PM, Ragozzino ME et al. Relative Timing Between Kappa Opioid Receptor Activation and Cocaine Determines the Impact on Reward and Dopamine Release. Neuropsychopharmacology 2016; 41(4): 989–1002. [PubMed: 26239494]

42. Johnson SW, North RA. Opioids excite dopamine neurons by hyperpolarization of local interneurons. J Neurosci 1992; 12(2): 483–488. [PubMed: 1346804]

43. Kudo T, Konno K, Uchigashima M, Yanagawa Y, Sora I, Minami M et al. GABAergic neurons in the ventral tegmental area receive dual GABA/enkephalin-mediated inhibitory inputs from the bed nucleus of the stria terminalis. Eur J Neurosci 2014; 39(11): 1796–1809. [PubMed: 24580812]

44. Korotkova TM, Brown RE, Sergeeva OA, Ponomarenko AA, Haas HL. Effects of arousal- and feeding-related neuropeptides on dopaminergic and GABAergic neurons in the ventral tegmental area of the rat. Eur J Neurosci 2006; 23(10): 2677–2685. [PubMed: 16817870]

45. van Zessen R, Phillips JL, Budygin EA, Stuber GD. Activation of VTA GABA neurons disrupts reward consumption. Neuron 2012; 73(6): 1184–1194. [PubMed: 22445345]

46. Kaufling J, Veinante P, Pawlowski SA, Freund-Mercier MJ, Barrot M. gamma-Aminobutyric acid cells with cocaine-induced DeltaFosB in the ventral tegmental area innervate mesolimbic neurons. Biol Psychiatry 2010; 67(1): 88–92. [PubMed: 19748079]

47. Jarvie BC, Hentges ST. Expression of GABAergic and glutamatergic phenotypic markers in hypothalamic proopiomelanocortin neurons. J Comp Neurol 2012; 520(17): 3863–3876. [PubMed: 22522889]

48. Wang D, He X, Zhao Z, Feng Q, Lin R, Sun Y et al. Whole-brain mapping of the direct inputs and axonal projections of POMC and AgRP neurons. Front Neuroanat 2015; 9: 40. [PubMed: 25870542]

49. Lutz PE, Kieffer BL. Opioid receptors: distinct roles in mood disorders. Trends Neurosci 2013; 36(3): 195–206. [PubMed: 23219016]

50. Komatsu H, Ohara A, Sasaki K, Abe H, Hattori H, Hall FS et al. Decreased response to social defeat stress in mu-opioid-receptor knockout mice. Pharmacol Biochem Behav 2011; 99(4): 676–682. [PubMed: 21703297]

51. Nikulina EM, Arrillaga-Romany I, Miczek KA, Hammer RP Jr. Long-lasting alteration in mesocorticolimbic structures after repeated social defeat stress in rats: time course of mu-opioid

receptor mRNA and FosB/DeltaFosB immunoreactivity. Eur J Neurosci 2008; 27(9): 2272–2284. [PubMed: 18445218]

52. Nikulina EM, Hammer RP Jr., Miczek KA, Kream RM. Social defeat stress increases expression of mu-opioid receptor mRNA in rat ventral tegmental area. Neuroreport 1999; 10(14): 3015–3019. [PubMed: 10549815]
53. Johnston CE, Herschel DJ, Lasek AW, Hammer RP Jr., Nikulina EM. Knockdown of ventral tegmental area mu-opioid receptors in rats prevents effects of social defeat stress: implications for amphetamine cross-sensitization, social avoidance, weight regulation and expression of brain-derived neurotrophic factor. Neuropharmacology 2015; 89: 325–334. [PubMed: 25446676]
54. Shanmugarajah L, Dunigan AI, Frantz KJ, Roseberry AG. Altered sucrose self-administration following injection of melanocortin receptor agonists and antagonists into the ventral tegmental area. Psychopharmacology (Berl) 2017; 234(11): 1683–1692. [PubMed: 28243712]
55. Yen HH, Roseberry AG. Decreased consumption of rewarding sucrose solutions after injection of melanocortins into the ventral tegmental area of rats. Psychopharmacology (Berl) 2015; 232(1): 285–294. [PubMed: 24985892]
56. Roseberry AG. Altered feeding and body weight following melanocortin administration to the ventral tegmental area in adult rats. Psychopharmacology (Berl) 2013; 226(1): 25–34. [PubMed: 23010797]
57. Zhan C, Zhou J, Feng Q, Zhang JE, Lin S, Bao J et al. Acute and long-term suppression of feeding behavior by POMC neurons in the brainstem and hypothalamus, respectively. J Neurosci 2013; 33(8): 3624–3632. [PubMed: 23426689]
58. Balthasar N, Dalgaard LT, Lee CE, Yu J, Funahashi H, Williams T et al. Divergence of melanocortin pathways in the control of food intake and energy expenditure. Cell 2005; 123(3): 493–505. [PubMed: 16269339]
59. Grupe DW, Nitschke JB. Uncertainty and anticipation in anxiety: an integrated neurobiological and psychological perspective. Nat Rev Neurosci 2013; 14(7): 488–501. [PubMed: 23783199]
60. Dietrich MO, Zimmer MR, Bober J, Horvath TL. Hypothalamic Agrp neurons drive stereotypic behaviors beyond feeding. Cell 2015; 160(6): 1222–1232. [PubMed: 25748653]
61. Burnett CJ, Li C, Webber E, Tsaousidou E, Xue SY, Bruning JC et al. Hunger-Driven Motivational State Competition. Neuron 2016; 92(1): 187–201. [PubMed: 27693254]
62. Padilla SL, Qiu J, Soden ME, Sanz E, Nestor CC, Barker FD et al. Agouti-related peptide neural circuits mediate adaptive behaviors in the starved state. Nat Neurosci 2016; 19(5): 734–741. [PubMed: 27019015]
63. Alhadeff AL, Su Z, Hernandez E, Klima ML, Phillips SZ, Holland RA et al. A Neural Circuit for the Suppression of Pain by a Competing Need State. Cell 2018; 173(1): 140–152 e115. [PubMed: 29570993]
64. Val-Laillet D, Aarts E, Weber B, Ferrari M, Quaresima V, Stoeckel LE et al. Neuroimaging and neuromodulation approaches to study eating behavior and prevent and treat eating disorders and obesity. Neuroimage Clin 2015; 8: 1–31. [PubMed: 26110109]
65. Kumar P, Goer F, Murray L, Dillon DG, Beltzer ML, Cohen AL et al. Impaired reward prediction error encoding and striatal-midbrain connectivity in depression. Neuropsychopharmacology 2018; 43(7): 1581–1588. [PubMed: 29540863]
66. Wagner G, de la Cruz F, Kohler S, Bar KJ. Treatment Associated Changes of Functional Connectivity of Midbrain/Brainstem Nuclei in Major Depressive Disorder. Sci Rep 2017; 7(1): 8675. [PubMed: 28819132]
67. Swann G, Byck GR, Dick DM, Aliev F, Latendresse SJ, Riley B et al. Effect of OPRM1 and stressful life events on symptoms of major depression in African American adolescents. J Affect Disord 2014; 162: 12–19. [PubMed: 24766998]
68. Madisen L, Zwingman TA, Sunkin SM, Oh SW, Zariwala HA, Gu H et al. A robust and high-throughput Cre reporting and characterization system for the whole mouse brain. Nat Neurosci 2010; 13(1): 133–140. [PubMed: 20023653]
69. Berglund ED, Liu C, Sohn JW, Liu T, Kim MH, Lee CE et al. Serotonin 2C receptors in pro-opiomelanocortin neurons regulate energy and glucose homeostasis. J Clin Invest 2013; 123(12): 5061–5070. [PubMed: 24177424]

70. Tong Q, Ye CP, Jones JE, Elmquist JK, Lowell BB. Synaptic release of GABA by AgRP neurons is required for normal regulation of energy balance. Nat Neurosci 2008.

71. Vong L, Ye C, Yang Z, Choi B, Chua S Jr., Lowell BB. Leptin action on GABAergic neurons prevents obesity and reduces inhibitory tone to POMC neurons. Neuron 2011; 71(1): 142–154. [PubMed: 21745644]

72. Balthasar N, Coppari R, McMinn J, Liu SM, Lee CE, Tang V et al. Leptin receptor signaling in POMC neurons is required for normal body weight homeostasis. Neuron 2004; 42(6): 983–991. [PubMed: 15207242]

73. Galassetti P, Tate D, Neill RA, Morrey S, Wasserman DH, Davis SN. Effect of sex on counterregulatory responses to exercise after antecedent hypoglycemia in type 1 diabetes. Am J Physiol Endocrinol Metab 2004; 287(1): E16–24. [PubMed: 14998785]

74. Atasoy D, Aponte Y, Su HH, Sternson SM. A FLEX switch targets Channelrhodopsin-2 to multiple cell types for imaging and long-range circuit mapping. J Neurosci 2008; 28(28): 7025–7030. [PubMed: 18614669]

75. Petreanu L, Huber D, Sobczyk A, Svoboda K. Channelrhodopsin-2-assisted circuit mapping of long-range callosal projections. Nat Neurosci 2007; 10(5): 663–668. [PubMed: 17435752]

76. Fan W, Boston BA, Kesterson RA, Hruby VJ, Cone RD. Role of melanocortinergic neurons in feeding and the agouti obesity syndrome. Nature 1997; 385(6612): 165–168. [PubMed: 8990120]

77. Fenalti G, Giguere PM, Katritch V, Huang XP, Thompson AA, Cherezov V et al. Molecular control of delta-opioid receptor signalling. Nature 2014; 506(7487): 191–196. [PubMed: 24413399]

78. Wu H, Wacker D, Mileni M, Katritch V, Han GW, Vardy E et al. Structure of the human kappa-opioid receptor in complex with JDTic. Nature 2012; 485(7398): 327–332. [PubMed: 22437504]

79. Spetea M, Schullner F, Moisa RC, Berzetei-Gurske IP, Schraml B, Dorfler C et al. Synthesis and biological evaluation of 14-alkoxymorphinans. 21. Novel 4-alkoxy and 14-phenylpropoxy derivatives of the mu opioid receptor antagonist cyprodime. J Med Chem 2004; 47(12): 3242–3247. [PubMed: 15163203]

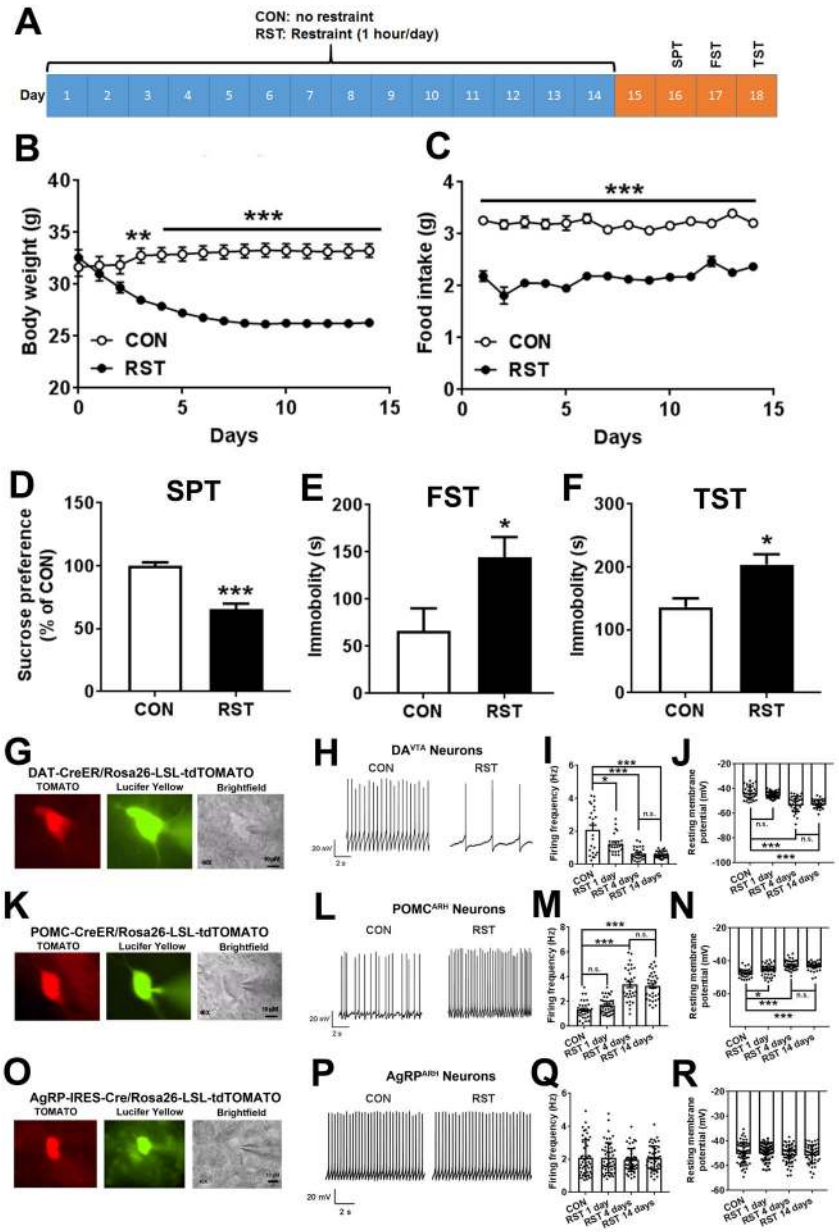

Figure 1. Chronic restraint stress induces metabolic and neurobehavioral deficits, and alters activity of DA^{VTA} and $POMC^{ARH}$ neurons.

(A) A diagram of restraint or control protocol followed by neurobehavioral tests. (B-C) Body weight (B) and food intake (C) measured daily during the 14-day restraint or control protocol. Results are shown as mean ± SEM. **, $P < 0.01$ and ***, $P < 0.001$ between RST *vs.* CON in two-way ANOVA analyses followed by Sidak post hoc test (N=7 mice per group). (D) Sucrose preference measured in the sucrose preference test on day 16. (E) Immobility time measured in the forced swim test on day 17. (F) Immobility time measured in the tail suspension test on day 18. Results are shown as mean ± SEM. *, $P < 0.05$ and **, $P < 0.01$ between RST *vs.* CON in t-tests (N=7 mice per group). (G) Representative microscopic images showing a recorded DA^{VTA} neuron (TOMATO-labelled in DAT-CreER/Rosa26-LSL-tdTOMATO mice). Scale bar= 10 μm. (H) Representative action potential

traces in DA^{VTA} neurons from mice subjected to CON or RST protocol for 4 days. (I-J) Quantifications of firing frequency (I) and resting membrane potential (J) in DA^{VTA} neurons from mice subjected to CON or RST protocol for 1, 4 or 14 days. Results are shown as mean ± SEM. *, $P < 0.05$ and ***, $P < 0.001$ between RST *vs.* CON in one-way ANOVA analyses followed by Tukey's test (N=24–30 neurons from 4 mice per group). (K) Representative microscopic images showing a recorded $POMC^{ARH}$ neuron (TOMATO-labelled in POMC-CreER/Rosa26-LSL-tdTOMATO mice). Scale bar= 10 μm. (L) Representative action potential traces in $POMC^{ARH}$ neurons from mice subjected to CON or RST protocol for 4 days. (M-N) Quantifications of firing frequency (M) and resting membrane potential (N) in $POMC^{ARH}$ neurons from mice subjected to CON or RST protocol for 1, 4 or 14 days. Results are shown as mean ± SEM. *, $P<0.05$ and ***, $P < 0.001$ between RST *vs.* CON in one-way ANOVA analyses followed by Tukey's test (N=33–40 neurons from 4 mice per group). (O) Representative microscopic images showing a recorded $AgRP^{ARH}$ neuron (TOMATO-labelled in AgRP-IRES-Cre/Rosa26-LSL-tdTOMATO mice). Scale bar= 10 μm. (P) Representative action potential traces in $AgRP^{ARH}$ neurons from mice subjected to CON or RST protocol for 4 days. (Q-R) Quantifications of firing frequency (Q) and resting membrane potential (R) in $POMC^{ARH}$ neurons from mice subjected to CON or RST protocol for 1, 4 or 14 days. Results are shown as mean ± SEM. N=46–49 neurons from 4 mice per group.

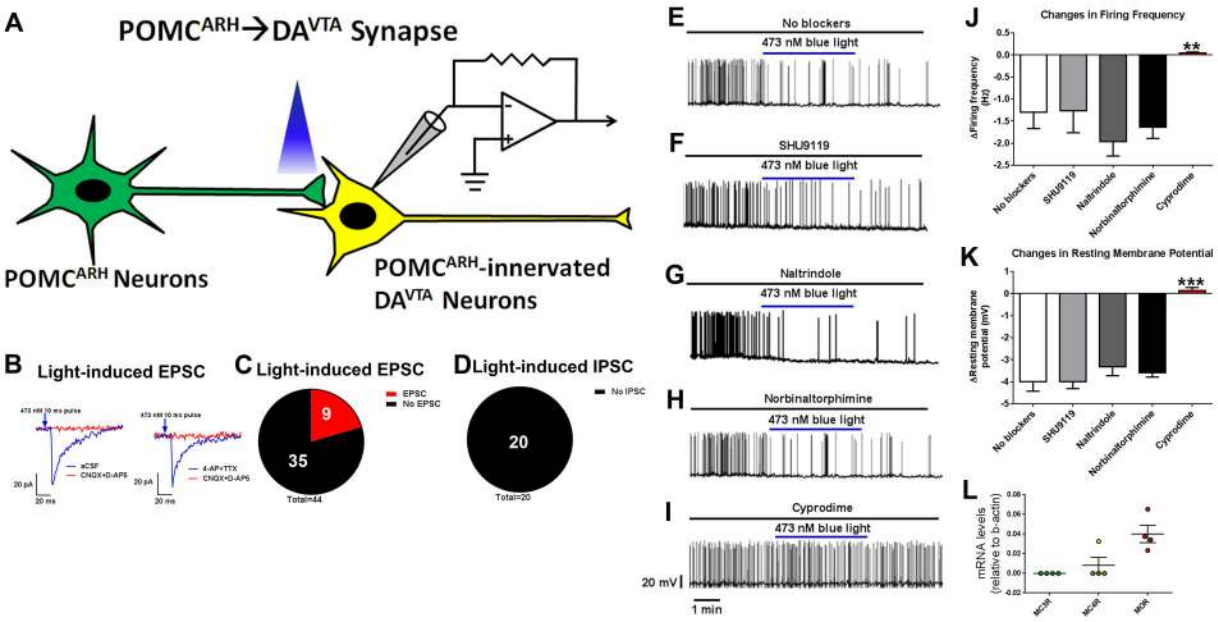

Figure 2. POMC^{ARH} neurons directly inhibit a portion of DA^{VTA} neurons via MOR-mediated mechanisms.

(A) Recordings in POMC^{ARH}-innervated DA^{VTA} neurons [GFP(+)TOMATO(+)] in response to photostimulation of ChR2-labelled POMC^{ARH}-originated fibers within the VTA. (B) Representative traces for light-evoked EPSC, which were blocked by 30 μM D-AP5 and 30 μM CNQX, but not affected by 400 μM 4-AP and 1 μM TTX. (C) The percentage of GFP(+)TOMATO(+) neurons that showed light-evoked EPSCs or no response. (D) The percentage of GFP(+)TOMATO(+) neurons that showed light-evoked IPSCs or no response. (E-I) Representative action potential traces in GFP(+)TOMATO(+) neurons in response to photostimulation of POMC^{ARH}-originated fibers within the VTA, in the absence (E) or presence of SHU9119 (50 μM, F), naltrindole (100 μM, G), norbinaltorphimine (100 μM, H), or cyprodime (200 μM, I). (J-K) Light-induced changes in firing frequency (J) and resting membrane potential (K). Results are shown as mean ± SEM. **, $P < 0.01$ and ***, $P < 0.001$ between cyprodime group vs. no blockers in one-way ANOVA analyses followed by Sidak post hoc test (N=10–19 neurons from 3 mice per group). (L) Relative mRNA levels of MC3R, MC4R and MOR in single VTA neurons labelled by both GFP and TOMATO. Results are shown as mean ± SEM with each data point plotted. N=4 neurons from 2 mice per group.

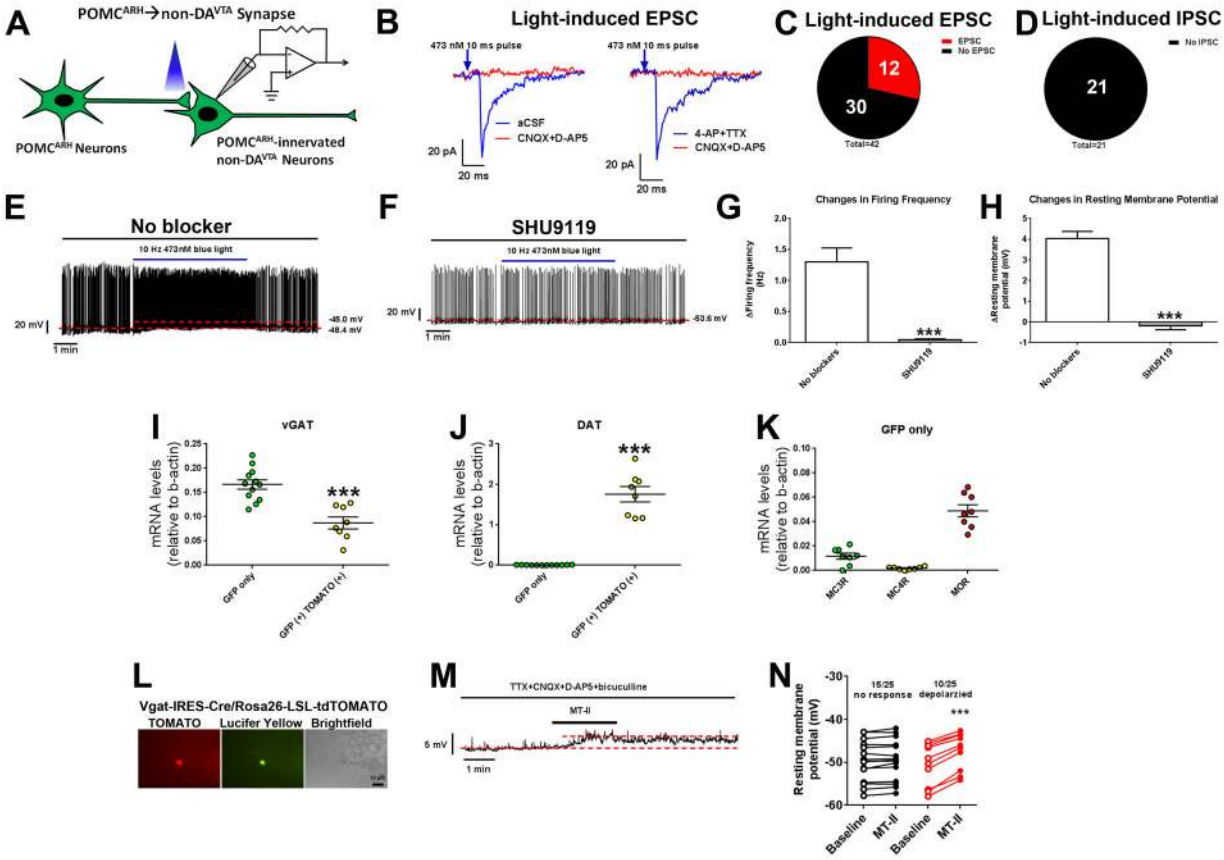

Figure 3. POMC^{ARH} neurons directly activate GABA^{VTA} neurons via MC3R-mediated mechanisms.

(A) Recordings in POMC^{ARH}-innervated non-DA^{VTA} neurons [GFP(+) only] in response to photostimulation of ChR2-labelled POMC^{ARH}-originated fibers within the VTA. (B) Representative traces for light-evoked EPSC, which were blocked by 30 μM D-AP5 and 30 μM CNQX, but not affected by 400 μM 4-AP and 1 μM TTX. (C) The percentage of GFP(+) neurons that showed light-evoked EPSCs or no response. (D) The percentage of GFP(+) neurons that showed light-evoked IPSCs or no response. (E-F) Representative action potential traces in GFP(+) neurons in response to photostimulation of POMC^{ARH}-originated fibers within the VTA, in the absence (E) or presence of SHU9119 (50 μM, F). (G-H) Light-induced changes in firing frequency (G) and resting membrane potential (H). Results are shown as mean ± SEM. N=10 neurons from 3 mice per group. ***, $P < 0.001$ between SHU9119 group vs. no blocker in t-tests. (I-J) Relative mRNA levels of vGAT (I) and DAT (J) in single VTA neurons labelled by GFP only or by both GFP and TOMATO. Results are shown as mean ± SEM with each data point plotted. ***, $P < 0.001$ between two groups in t-tests (N=8 or 12 neurons from 2 mice per group). (K) Relative mRNA levels of MC3R, MC4R and MOR in single VTA neurons labelled by GFP only. Results are shown as mean ± SEM with each data point plotted. N=8 neurons from 2 mice per group. (L) Representative microscopic images showing a recorded GABA^{VTA} neuron (TOMATO-labelled in Vgat-IRES-Cre/Rosa26-LSL-tdTOMATO mice). Scale bar= 10 μm. (M) Representative traces for resting membrane potential recorded in a GABA^{VTA} neuron depolarized by 300 nM MT-II

in the presence of 1 μM TTX, 30 μM CNQX, 30 μM D-AP5 and 50 μM bicuculline. (N) The resting membrane potential at the baseline and after MT-II treatment. Results are shown as individual data point. ***, $P < 0.001$ between baseline vs. MT-II in paired t-tests (N=10 or 15 neurons from 2 mice per group).

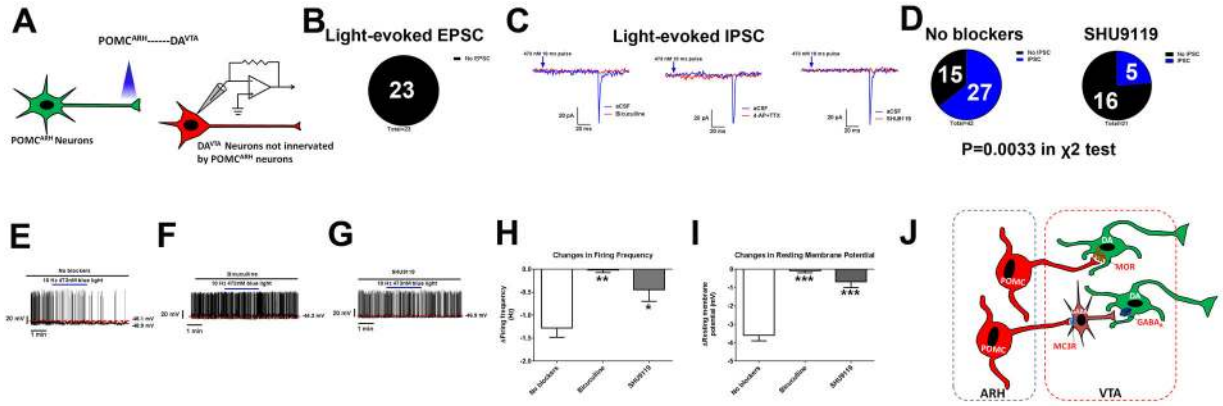

Figure 4. POMC^{ARH} neurons indirectly inhibit a subset of DA^{VTA} neurons.

(A) Recordings in DA^{VTA} neurons not innervated by POMC^{ARH} neurons [TOMATO(+) only] in response to photostimulation of ChR2-labelled POMC^{ARH}-originated fibers within the VTA. (B) The percentage of TOMATO(+) neurons that showed light-evoked EPSCs or no response. (C) Representative traces for light-evoked IPSC, which were blocked by 50 μM bicuculline, by 400 μM 4-AP and 1 μM TTX, or by 50 μM SHU9119. (D) The percentage of TOMATO(+) neurons that showed light-evoked IPSCs or no response in conditions with no blockers or with SHU9119. P=0.0033 in $\chi 2$ test. (E-G) Representative action potential traces in TOMATO(+) neurons in response to photostimulation of POMC^{ARH}-originated fibers within the VTA, in the absence (E) or presence of bicuculline (50 μM, F), or SHU9119 (50 μM, G). (H-I) Light-induced changes in firing frequency (H) and resting membrane potential (I). Results are shown as mean ± SEM. *, $P<0.05$, **, $P<0.01$ or ***, $P < 0.001$ between other group vs. no blocker in one-way ANOVA analyses followed by Sidak post hoc tests (N=11 to 24 neurons from 3 mice per group). (J) A schematic model for POMC^{ARH} neurons to directly or indirectly inhibit different subsets of DA^{VTA} neurons.

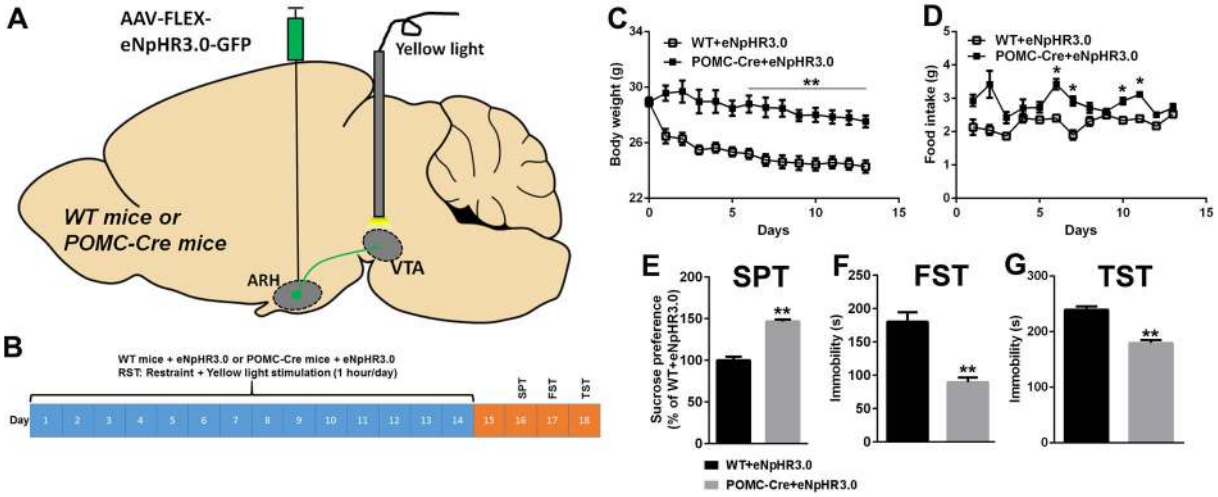

Figure 5. Photoinhibition of the POMC^{ARH}→VTA circuit increases food intake and decreases anhedonia and depression in mice exposed to chronic restraint stress.

(A) Schematic experimental strategy using the AAV-FLEX-eNpHR3.0-EYFP virus to inhibit the POMC^{ARH}→VTA circuit. (B) The experimental protocol for 14-day restraint with or without photoinhibition of the POMC^{ARH}→VTA circuit followed by neurobehavioral tests. (C-D) Body weight (C) and food intake (D) measured daily during the 14-day restraint protocol. Results are shown as mean ± SEM. *, $P < 0.05$ and **, $P < 0.01$ between WT *vs.* POMC-Cre mice in two-way ANOVA analyses followed by Sidak post hoc test (N=5 or 6 mice per group). (E) Sucrose preference measured in the sucrose preference test on day 16. (F) Immobility time measured in the forced swim test on day 17. (G) Immobility time measured in the tail suspension test on day 18. Results are shown as mean ± SEM. **, $P < 0.01$ between WT *vs.* POMC-Cre mice in t-tests (N=5–6 mice per group).